



# Performance enhancement of heat exchangers using eccentric tape inserts and nanofluids

Navid Moghaddaszadeh<sup>1</sup> · Javad Abolfazli Esfahani<sup>1</sup> · Omid Mahian<sup>2,3</sup>

Received: 8 September 2018 / Accepted: 3 January 2019 / Published online: 19 January 2019  
© Akadémiai Kiadó, Budapest, Hungary 2019

## Abstract

Optimizing the performance of solar collectors and photovoltaic thermal systems that are used for heating/cooling of building as well as electricity generation will efficiently help to approach zero-energy buildings. For this purpose, improving the efficiency of heat exchangers as the main part of solar collectors and photovoltaic thermal systems is necessary. In this paper, two passive methods are employed to ameliorate the efficiency of heat exchangers. To do this, the effect of using Al<sub>2</sub>O<sub>3</sub>/water nanofluid in a heat exchanger tube with a swirling flow turbulator was studied. A numerical simulation was carried out to obtain thermal–hydraulic performance in the tube with eccentric helical screw-tape turbulators. The influences of different parameters including nanoparticles volume fraction and eccentricity of tube insert on the performance of heat exchanger are investigated. The results reveal that the coefficient of heat transfer enhances approximately 4.5 times by using nanofluid at nanoparticles volume fraction of 4% with helical turbulator compared to the plain tube at nanoparticles volume fraction of 0%. It was also found that the value of Performance Evaluation Criterion ameliorates as the nanoparticle loading increases. The maximum value of Performance Evaluation Criterion reached 2.2 at nanoparticles volume fraction of 4%, Reynolds number of 4000 and eccentricity of 3. The results of this study reveal the potential of the suggested technique to enhance various thermal systems including solar collectors.

**Keywords** Nanofluid · Helical screw-tape turbulator · Heat exchanger · Solar collectors

## List of symbols

|       |  |
|-------|--|
| $C_p$ | Specific heat capacity (J kg <sup>-1</sup> K <sup>-1</sup> )   |
| $d_1$ | Internal diameter of helical screw-tape (m)                    |
| $d_2$ | Outer diameter of helical screw-tape (m)                       |
| $D$   | Tube diameter (m)  |
| $e$   | Eccentricity (mm)  |
| $E$   | Total energy (m <sup>2</sup> s <sup>-2</sup> )                 |
| $f$   | Friction factor (–)  |
| $h$   | Heat transfer coefficient (W m <sup>-2</sup> K <sup>-1</sup> ) |
| $L$   | Tube length (m)  |
| $Nu$  | Nusselt number (–)   |

|           |  |
|-----------|--|
| $P$       | Pressure (Pa)                                      |
| $p$       | Twist pitch  |
| $Pr$      | Prandtl number (–) ( $Pr = \nu/\alpha$ )           |
| $PR$      | Pitch ratio (–)                                    |
| $q$       | Heat flux (W m <sup>-2</sup> )                     |
| $r$       | Tube radius (m)                                    |
| $Re$      | Reynolds number (–) ( $Re = \rho U_{in} D/\mu$ )   |
| $T$       | Temperature (K)                                    |
| $\dot{V}$ | Volume flow rate (m <sup>3</sup> s <sup>-1</sup> ) |

## Greek symbols

|           |   |
|-----------|---|
| $\delta$  | Kronecker delta function (–)                              |
| $\lambda$ | Thermal conductivity (W m <sup>-1</sup> K <sup>-1</sup> ) |
| $\mu$     | Dynamic viscosity (kg m <sup>-1</sup> s <sup>-1</sup> )   |
| $\rho$    | Density of the fluid (kg m <sup>-3</sup> )                |
| $\sigma$  | Turbulent Prandtl number (–)                              |
| $\tau$    | Wall shear stress (kg m <sup>-1</sup> )                   |
| $\phi$    | Nanoparticle concentration (–)                            |

## Subscripts/superscripts

|      |               |
|------|---------------|
| $e$  | Enhanced tube |
| $in$ | Inlet         |

✉ Javad Abolfazli Esfahani  
abolfazl@um.ac.ir

<sup>1</sup> Department of Mechanical Engineering, Ferdowsi University of Mashhad, Mashhad 91775-1111, Iran

<sup>2</sup> School of Chemical Engineering and Technology, Xi'an Jiaotong University, Xi'an 710049, Shaanxi, China

<sup>3</sup> Center for Advanced Technologies, Ferdowsi University of Mashhad, Mashhad, Iran

$m$  Average  
 0 Smooth tube

### Abbreviations

HE Heat exchanger  
 HTC Heat transfer coefficient  
 NF Nanofluid  
 NP Nanoparticle  
 PEC Performance evaluation criterion  
 SST Shear stress transport

## Introduction

Approaching zero-energy buildings will save the fossil sources in one hand, and on the other hand, will reduce global warming and CO<sub>2</sub> emission [1, 2]. The efficacy optimization of solar collectors and photovoltaic thermal (PV/T) systems which could be used for heating/cooling of building as well as electricity generation will efficiently help to approach zero-energy buildings [3, 4]. To do this, improving the efficiency of heat exchangers (HEs) as the main part of solar collectors and PV/T systems is necessary.

In the present study, two passive methods are employed to ameliorate the efficiency of HEs. The first technique is the use of a helical screw-tape turbulator with different eccentricities, and the second method is the nanoparticles (NPs) addition to the working fluid flowing in the HE. Here, a brief review of some studies in this subject is done. Bellos and Tzivanidis [5] examined the influence of equipping a solar collector with a star-shaped fin. They conducted energy and exergy examination for the system and found the optimal structure of the star-shaped fin. Bhattacharyya et al. [6] modeled a solar heater with twisted tape turbulators for both turbulent and laminar regimes. They concluded that as the twist ratio reduces the rate of heat exchange and pressure drop increase dramatically. They reported that the performance index declines with increasing Reynolds number ( $Re$ ). Song et al. [7] employed helical screw-tape inserts around the absorber tube outer surface in turbulent flow to improve the thermal efficiency. Sheikholeslami et al. [8] examined discontinuous helical turbulators experimentally. Considering that they had chosen many different parameters like pitch ratio, open area ratio and  $Re$  number, so they used a genetic algorithm to find the optimal design of HE. They stated that the Nusselt number ( $Nu$ ) augmentation is more evidence with decreasing pith ratio, but friction factor ( $f$ ) goes up too. The open area ratio's effect is interesting because it has not any sensible change on Nusselt number but it decreases friction factor very well (reduction by three and four times);

therefore, it leads to increase PEC. Chang et al. [9] studied concentric and eccentric tube inserts in receiver tubes. They showed that the usage of these tube inserts enhances the heat transfer performance, especially in the eccentric case. Lim et al. [10] studied the influence of twisted tapes on the performance of an HE under laminar regime. They evaluated the performance of the HE according to various performance indices including the ratio of heat transfer augmentation, pumping power, flow resistance,  $Nu$ , and heat duty. They reported that using the turbulators can enhance  $Nu$  up to 3 times while  $f$  rises by 10 times compared with the plain tube. The value of PEC was achieved between 0.9 and 3, depends on the pumping power value. The effect of simple helical screw-tape on the efficiency of thermal tubes was studied experimentally by Eiamsa-ard and Promvonge [11]. Zhang et al. [12] studied this type of inserts numerically. They analyzed helical screw-tapes by two efficiency criteria based on the entropy generation minimization principle and physical quantity synergy principle. Rashidi et al. [13] studied helical screw-tapes from the second law of thermodynamic viewpoint. Liu et al. [14] evaluated the effect of using a new twisted tape insert in laminar flow. They concluded that  $Nu$  and PEC increased by 151–195% and 90–123% of the simple twisted tape, respectively. They concluded that using turbulators follows with a thinner thermal boundary layer. Consequently, it leads to a higher gradient of temperature in the vicinity of the tube wall. Moghaddaszadeh et al. [15] evaluated the impact of an eccentric helical screw-tape on the effectiveness of an HE tube where the working fluid was water. It was found that the performance of the HE enhances when the tapes with higher eccentricity are used.

Adding NPs to conventional fluids has been used as another passive technique to enhance the heat transfer rate. Many studies have been done on nanofluids (NFs), and the readers can refer to some recent research and review articles on the application and modeling of NFs [16–24].

Simultaneous application of both insert tubes and NFs has been investigated in some studies which a brief review of them is presented here. Sunder et al. [25] investigated a solar water heater with combining twisted tape and NFs. They used Al<sub>2</sub>O<sub>3</sub>/water NF as the working fluid in different concentrations and twisted tape turbulators with twist ratios of 5–15. They reported that the collector efficiency increased with NF concentration and decreased with the twist ratio. In another experimental study, Sunder et al. [26] investigated the influence of using longitudinal strip turbulators along with nanodiamond–nickel hybrid NF. They concluded that  $Re = 22,000$  using hybrid NF with 0.3% volume concentration leads to 93.30% enhancement in Nusselt number and 125% increase in friction factor.

Sheikholeslami et al. [27] studied the simultaneous application of CuO/water NF and helical twisted tape

turbulator inside a tube, numerically. They showed that HTC augments with raising  $Re$ .

Esmailzadeh et al. [28] investigated the influence of twisted tape thickness in the presence of  $\gamma\text{-Al}_2\text{O}_3/\text{water}$  NF experimentally. They examined three thickness values of 0.5 mm, 1 mm and 2 mm in laminar flow regime. They showed that thicker twisted tape is more effective for increasing heat transfer, while it leads to pressure drop increase. They deduced that the highest enhancement of the HE was achieved at maximum values of thickness and volume concentration.

Sheikholeslami et al. [29] investigated CuO/water NF impact on the exergy loss inside a tube equipped with modified twisted tape. They showed that higher revolution angle and  $Re$  make the thermal boundary layer thinner. Exergy loss reduces with the increase in Reynolds number and with ratio. Bellos et al. [30] studied CuO/water NF flow in a finned collector tube. They showed that using internal fins is more useful for heat transfer enhancement compared to NFs, while combining these methods gives the best results based on thermal criteria. According to their results, the thermal augmentation with NF reached by 0.76%, by means of internal fins up to 1.1% and by both NF and fins about 1.54%.

Akyurek et al. [31] studied  $\text{Al}_2\text{O}_3/\text{water}$  NF in a tube equipped with wire coil turbulator. They revealed that  $Nu$  augmented with increasing the particle concentration and  $Re$ . They showed that  $Nu$  enhances up to 35.66–168.26% for concentrations between 0.4 and 1.6%, in comparison with pure water. Due to the considerable pressure drop of wire coil turbulators and negligible pressure drop of NF, they concluded that it is more advantageous to use NFs as the passive technique for heat transfer enchantment instead of turbulator. Zheng et al. [32] used  $\text{Al}_2\text{O}_3/\text{water}$  NF in a tube fitted with dimpled twisted tapes numerically. Their results showed that the swirl flow intensity increases at the tube center and in the vicinity of the tube wall, which leads to the enhancement of secondary flow, flow mixing and heat transfer. The values of PEC were between 1.1 and 1.6, and it decreased with an increase in Reynolds number. They showed that dimples led to HTC growth by 25.53% compared to the plain tape. A comprehensive review on the combination of nanofluids and inserts has been done by Rashidi et al. [33].

The literature review shows there is no study on the combined usage of eccentric helical screw-tape turbulator and NFs in heat exchanger tubes. In this study, we investigate the influence of using  $\text{Al}_2\text{O}_3/\text{water}$  NF with an eccentric helical screw-tape insert. The effects of different parameters such as eccentricity value, NF concentration, and  $Re$  on the system performance are assessed numerically. To achieve a correct comparison between different cases, Performance Evaluation Criterion (PEC) is used.

## Problem description

The geometry and coordinate system for the simulated tube heat exchanger are depicted in Fig. 1.  $\text{Al}_2\text{O}_3/\text{water}$  NF with fully developed inlet velocity and temperature of 353 K flows through a three-dimensional tube with a diameter of  $D$  and a length of  $L$ . An eccentric helical screw-tape with outer diameter of  $d_2$ , inner diameter of  $d_1$ , thickness  $t$ , pitch ratio of PR and eccentricity of “ $e$ ” are mounted inside the tube. This helical insert is disclosed in Fig. 1. The pitch ratio is described as the ratio of one twist pitch ( $p$ ) to the tube diameter ( $D$ ). The assumptions in the study are:

- The flow is 3D, steady and incompressible in turbulence regime.
- NF was modeled as a single-phase liquid. Albojamal and Vafai [34] compared single-phase and two-phase approaches to predict the NF characteristics and found that the single-phase model can estimate NFs characteristics accurately. All the effective properties of the  $\text{Al}_2\text{O}_3/\text{water}$  NF are presented in Table 1. The equations used for calculating these properties of NF can be found at [35].
- All simulations have been conducted for three values of eccentricity including  $e = 0, 2$  and  $3$ ,  $0 < \varphi < 4\%$ , a fixed value of the pitch ratio PR = 18 mm, and  $Re$  in the range of 4000–12,000. Moreover, the tube has a length of 1 m, and a diameter of 0.025 mm. Inner and outer diameters of helical screw-tape are fixed at  $d_1 = 0.005$  and  $d_2 = 0.017$  m. Geometrical parameters are defined in Table 2.

## Mathematical model

### Governing equations

By considering the turbulent flow in the HE, the governing equations become [36]:

- Mass conservative:

$$\frac{\partial}{\partial x_i} (\rho_{\text{eff}} u_i) = 0 \quad (1)$$

- Momentum:

$$\begin{aligned} \frac{\partial \rho_{\text{eff}} u_i}{\partial t} + \frac{\partial}{\partial x_j} (\rho_{\text{eff}} u_i u_j) = & -\frac{\partial P}{\partial x_i} \\ & + \frac{\partial}{\partial x_j} \left[ \mu_{\text{eff}} \left( \frac{\partial u_i}{\partial x_j} + \frac{\partial u_j}{\partial x_i} - \frac{2}{3} \delta_{ij} \frac{\partial u_k}{\partial x_k} \right) \right] \\ & + \frac{\partial}{\partial x_j} \left( -\rho_{\text{eff}} \overline{u'_i u'_j} \right) \end{aligned} \quad (2)$$

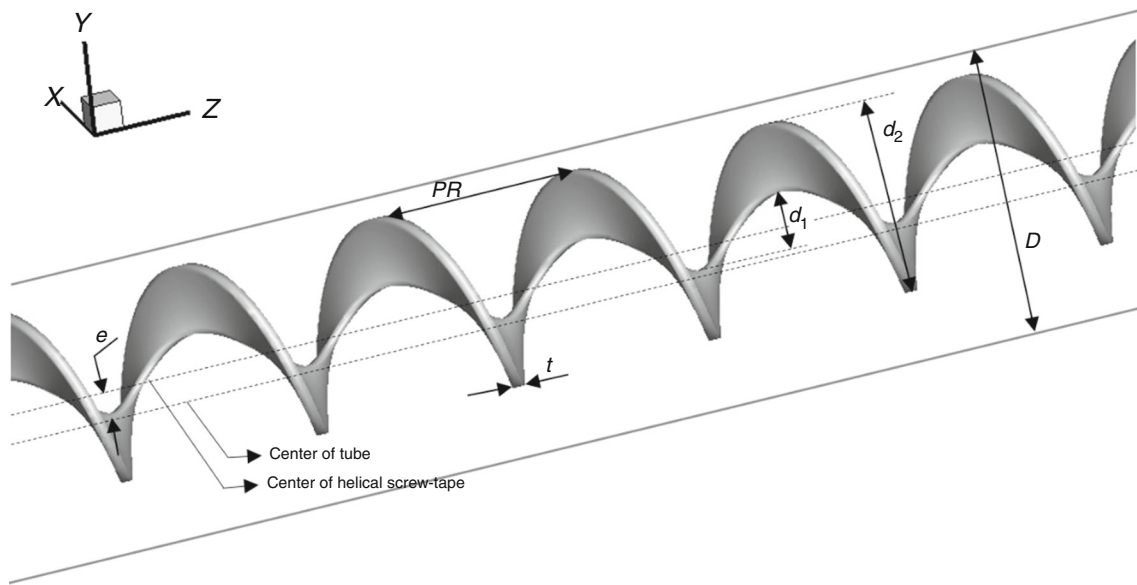


Fig. 1 Computational domain with coordinate system

Table 1 Effective properties of Al<sub>2</sub>O<sub>3</sub>/water nanofluid at 348 K

| $\phi$   | 0%       | 1%       | 2%       | 3%       | 4%       |
|--|----------|----------|----------|----------|----------|
| $\rho_{\text{eff}}/\text{kg m}^{-3}$                 | 974.86   | 1003.91  | 1032.96  | 1062.02  | 1091.07  |
| $C_{p,\text{eff}}/\text{J kg}^{-1} \text{K}^{-1}$    | 4192     | 4157.55  | 4123.29  | 4086.02  | 4054.75  |
| $\lambda_{\text{eff}}/\text{W m}^{-1} \text{K}^{-1}$ | 0.667    | 0.815    | 0.966    | 1.121    | 1.278    |
| $\mu_{\text{eff}}/\text{kg m}^{-1} \text{s}^{-1}$    | 0.000378 | 0.000387 | 0.000397 | 0.000406 | 0.000420 |

Table 2 Values of geometrical parameters

|   |                                      |
|---|--------------------------------------|
| Tube length                             | $L = 1 \text{ m}$                    |
| Tube diameter                           | $D = 0.025 \text{ m}$                |
| Internal diameter of helical screw-tape | $d_1 = 0.005 \text{ m}$              |
| Outer diameter of helical screw-tape    | $d_2 = 0.017 \text{ m}$              |
| Pitch ratio                             | $PR = p/D = 18 \text{ mm}$           |
| Eccentricity                            | $e = 0, 2 \text{ and } 3 \text{ mm}$ |

where  $P$  is pressure,  $\delta_{ij}$  stands for Kronecker delta function, and  $u'$  is fluctuated velocity. Moreover,  $\overline{\rho_{\text{eff}} u'_i u'_j}$  is the Reynolds stress.

• Energy:

$$\frac{D}{Dt}[(\rho_{\text{eff}} E)] = \frac{\partial}{\partial x_j} \left[ \left( \lambda_{\text{eff}} + \frac{C_{p,\text{eff}} \mu_t}{Pr_t} \right) \frac{\partial T}{\partial x_j} + u_i (\tau_{ij})_{\text{eff}} \right] \quad (3)$$

Subscript “t” denotes turbulent. Also,  $E = C_{p,\text{eff}} T + \left( \frac{P}{\rho_{\text{eff}}} \right) + \left( \frac{u^2}{2} \right)$ , and

$$(\tau_{ij})_{\text{eff}} = \mu_{\text{eff}} \left( \frac{\partial u_j}{\partial x_i} + \frac{\partial u_i}{\partial x_j} \right) - \frac{2}{3} \mu_{\text{eff}} \frac{\partial u_i}{\partial x_j} \delta_{ij} \quad (4)$$

A SST  $k - \omega$  turbulence model is considered for this problem. The transport equations for SST  $k - \omega$  model are:

$$\frac{D}{Dt}(\rho_{\text{eff}} k u_i) = \frac{\partial}{\partial x_j} \left( \Gamma_k \frac{\partial k}{\partial x_j} \right) + \tilde{G}_k - Y_k + S_k \quad (5)$$

$$\frac{D}{Dt}(\rho_{\text{eff}} \omega k u_i) = \frac{\partial}{\partial x_j} \left( \Gamma_\omega \frac{\partial \omega}{\partial x_j} \right) + G_\omega - Y_\omega + D_\omega + S_\omega \quad (6)$$

in the above,  $k$  stands for turbulent kinetic energy. In addition,  $\Gamma_k$  and  $\Gamma_\omega$  indicate the effective diffusivity of  $k$  and  $\omega$  parameters, respectively.  $Y_\omega = \rho_{\text{eff}} \beta \omega^2$  and  $Y_k = \rho_{\text{eff}} \beta^* k \omega$  and  $G_k = -\rho_{\text{eff}} u'_i u'_j \left( \frac{\partial u_j}{\partial x_i} \right)$  are the generation of turbulence kinetic energy created by the averaged velocity gradients and  $G_\omega$  is the generation of  $\omega$ .  $\tilde{G}_k$  and  $G_\omega$  are calculated by:

$$\tilde{G}_k = \min(G_k, 10 \beta^* k \omega) \quad (7)$$

$$G_\omega = \frac{\alpha}{\nu_\tau} G_k \quad (8)$$

where  $\nu_\tau$  stands for kinematic turbulent viscosity and  $\beta^*$  is a constant. In addition, heat diffusion coefficient ( $\alpha$ ) can be calculated by:

$$\alpha = \alpha_\infty \frac{\left(\alpha_0^* + \frac{Re_t}{R_\omega}\right)}{\left(1 + \frac{Re_t}{R_\omega}\right)} \tag{9}$$

where  $Re_t = \frac{\rho k}{\mu \omega}$ ,  $R_\omega = 2.95$ , and  $\alpha_0^* = \frac{\beta_i}{3}$ .  $\alpha_\infty$  is calculated by:

$$\alpha_\infty = F_1 \alpha_{\infty,1} + (1 - F_1) \alpha_{\infty,2} \tag{10}$$

where  $F$  is blending equation.  $\alpha_{\infty,1}$  and  $\alpha_{\infty,2}$  can be calculated by:

$$\alpha_{\infty,1} = \frac{\beta_{i,1}}{\beta_\infty^*} - \frac{\kappa^2}{\sigma_{\omega,1} \sqrt{\beta_\infty^*}} \tag{11}$$

$$\alpha_{\infty,2} = \frac{\beta_{i,2}}{\beta_\infty^*} - \frac{\kappa^2}{\sigma_{\omega,2} \sqrt{\beta_\infty^*}} \tag{12}$$

where  $\Gamma_k$  and  $\Gamma_\omega$  are:

$$\Gamma_k = \mu + \frac{\mu_t}{\sigma_k} \tag{13}$$

$$\Gamma_\omega = \mu + \frac{\mu_t}{\sigma_\omega} \tag{14}$$

$$\sigma_k = \frac{1}{\frac{F_1}{\sigma_{k,1}} + \frac{(1-F_1)}{\sigma_{k,2}}} \tag{15}$$

$$\sigma_\omega = \frac{1}{\frac{F_1}{\sigma_{\omega,1}} + \frac{(1-F_1)}{\sigma_{\omega,2}}} \tag{16}$$

in the above,  $\mu_t$  is turbulent viscosity and can be written as:

$$\mu_t = \alpha^* \frac{\rho k}{\omega} \tag{17}$$

$\alpha^*$  is the turbulent viscosity calculated by:

$$\alpha^* = \alpha_\infty^* \frac{\left(\alpha_0^* + \frac{Re_t}{R_k}\right)}{\left(1 + \frac{Re_t}{R_k}\right)} \tag{18}$$

where  $Re_t = \frac{\rho k}{\mu \omega}$ ,  $R_k = 6$ ,  $\alpha_0^* = \frac{\beta_i}{3}$ , and  $\beta_i = 0.072$ .  $\alpha_\infty^* = 1$  is employed for large value of Reynolds number.  $F_1$  is calculated by:

$$F_1 = \tan(\Phi_1^4) \tag{19}$$

where  $\Phi_1$  is defined by:

$$\Phi_1 = \min \left[ \max \left( \frac{\sqrt{k}}{0.09 \omega y}, \frac{500 \mu}{\rho y^2 \omega} \right), \frac{4 \rho k}{\sigma_{\omega,2} D_\omega^+ y^2} \right] \tag{20}$$

where  $D_\omega^+$  is positive portion of the cross-diffusion term calculated by:

$$D_\omega^+ = \max \left[ 2 \rho \frac{1}{\sigma_{\omega,2}} \frac{1}{\omega} \frac{\partial k}{\partial x_j} \frac{\partial \omega}{\partial x_j}, 10^{-10} \right] \tag{21}$$

$\beta_i$  and  $D_\omega$  are given by:

$$\beta_i = F_1 \beta_{i,1} + (1 - F_1) \beta_{i,2} \tag{22}$$

$$D_\omega = 2(1 - F_1) \rho \sigma_{\omega,2} \frac{1}{\omega} \frac{\partial k}{\partial x_j} \frac{\partial \omega}{\partial x_j} \tag{23}$$

The SST  $k - \omega$  model constants [37] are available in Table 3.

The Performance Evaluation Criterion (PEC) was specified for various enhancement methods in Ref. [38]. Because of the Fixed Geometry-2 case was validated for the helical screw-tape turbulators, the same case was used to assess thermal performance in this study. The HTC and  $f$  of the plain tube and tube fitted with helical screw-tape turbulators and NF are considered under the same pumping power for Fixed Geometry-2 case as given below [38].

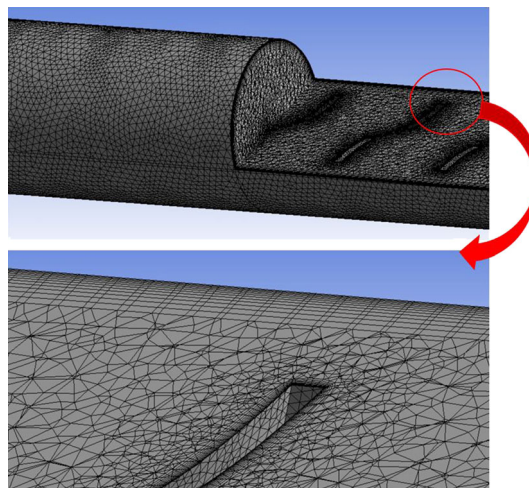


Fig. 2 Sample mesh inside the tube

Table 3 SST k-omega model constant [37]

|                        |                         |                         |                             |                   |                          |
|------------------------|-------------------------|-------------------------|-----------------------------|-------------------|--------------------------|
| $\sigma_{k,1} = 1.176$ | $\sigma_{k,2} = 1.0$    | $\sigma_{\omega,1} = 2$ | $\sigma_{\omega,2} = 1.168$ | $\alpha_1 = 0.31$ | $\beta_{i,1} = 0.075$    |
| $\beta_{i,2} = 0.0828$ | $\alpha_\infty^* = 1.0$ | $\alpha_\infty = 0.52$  | $\beta_\infty^* = 0.09$     | $\beta_i = 0.072$ | $\alpha_0 = \frac{1}{9}$ |
| $R_\beta = 8.0$        | $R_k = 6.0$             | $R_\omega = 2.95$       | $\zeta^* = 1.5$             | $\sigma_k = 2.0$  | $\sigma_\omega = 2.0$    |

$$(\dot{V}\Delta P)_0 = (\dot{V}\Delta P)_e \tag{24}$$

$$(fRe^3)_0 = (fRe^3)_e \tag{25}$$

$$Re_0 = Re_e \left(\frac{f_e}{f_0}\right)^{1/3} \tag{26}$$

The PEC is presented as follows [39]:

$$PEC = \left(\frac{Nu_e}{Nu_0}\right) \left(\frac{f_0}{f_e}\right)^{1/3} \tag{27}$$

where subscript 0 denotes a smooth tube (no helical screw-tape turbulator) where water (base fluid) is flowing in it, and e denotes an enhanced tube. In Eq. (24), the pressure drop ( $\Delta P$ ) is proportional to  $u^2$  and  $Re^2$ . Also, the volume

flow rate ( $\dot{V}$ ) is proportional to  $u$  and  $Re$ . The friction factor ( $f$ ) in Eq. (27) is calculated by:

$$f = 2\Delta p \frac{D_h}{L} \frac{1}{\rho u_m^2} \tag{28}$$

where  $u_m$  is the average velocity, defined by:

$$u_m = \frac{1}{R} \int_0^R u dr \tag{29}$$

The heat transfer coefficient in Eq. (27) can be calculated by:

$$h = \frac{q''}{T_w - T_m} \tag{30}$$

where  $T_m$  is bulk temperature defined by:

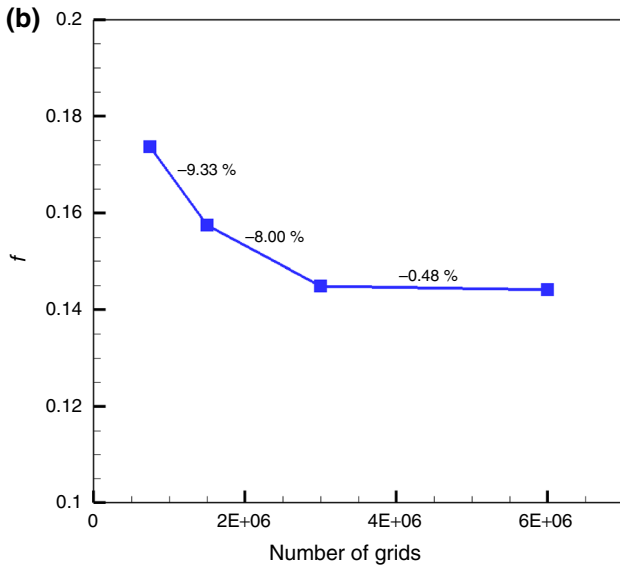
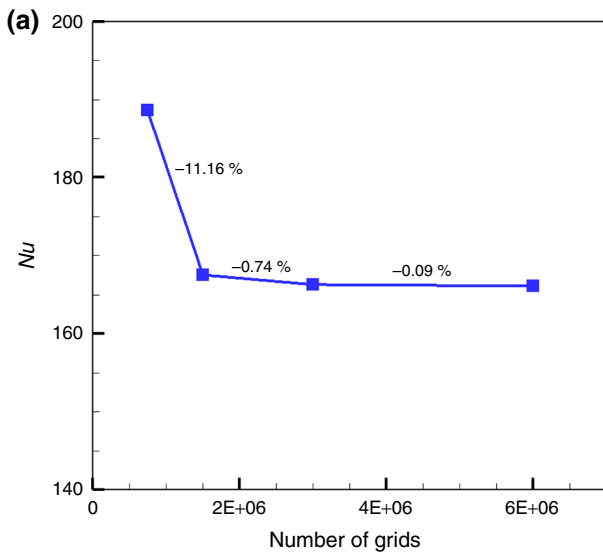


Fig. 3 The results of grid independence test **a** for  $Nu$ , and **b** friction factor

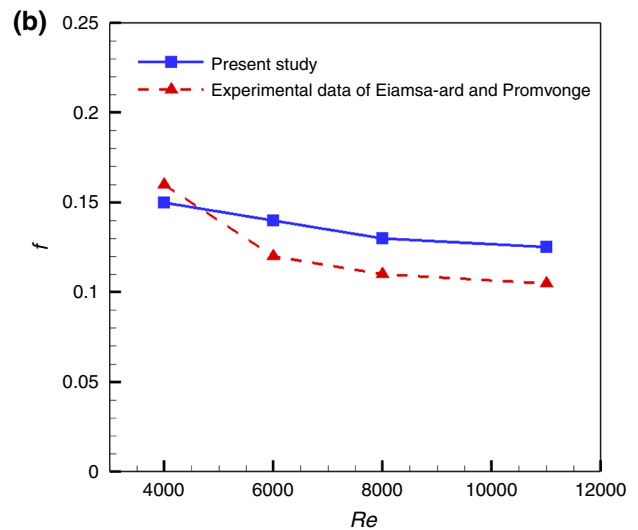
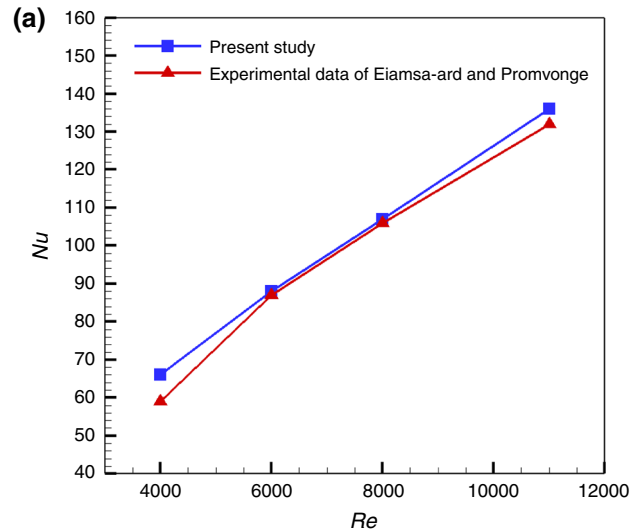


Fig. 4 Comparison between the current numerical results and experimental data [11] for  $e = 0$ , **a**  $Nu$  and **b** friction factor



$$T_m = \frac{\int_0^R uTrdr}{\int_0^R urdr} \tag{31}$$

The Nusselt number defined by:

$$Nu = \frac{hD}{\lambda} \tag{32}$$

### Boundary conditions

To solve the governing equations, we need to define appropriate boundary conditions. The boundary conditions are as follows:

- Inlet (fully developed velocity and fixed temperature):  
 $u = U_{fd}, v = 0, w = 0, T = 353 \text{ K}, k = k_{in}, \omega = \omega_{in}$  (33)
- Tube surfaces (Constant temperature and no-slip boundary conditions):

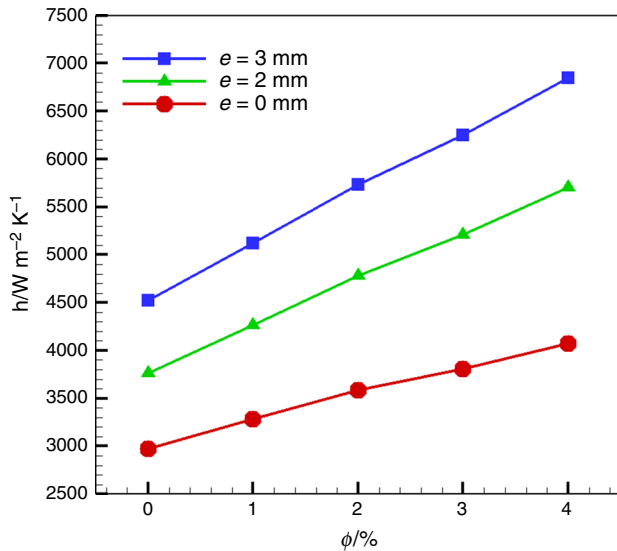


Fig. 5 Variations of heat transfer coefficient with  $\phi$  at  $Re = 12,000$

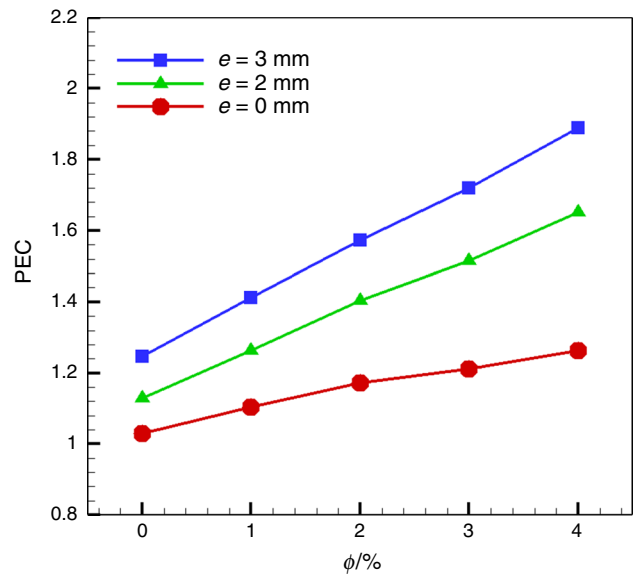


Fig. 7 Variations of PEC with  $\phi$  for different cases at  $Re = 12,000$

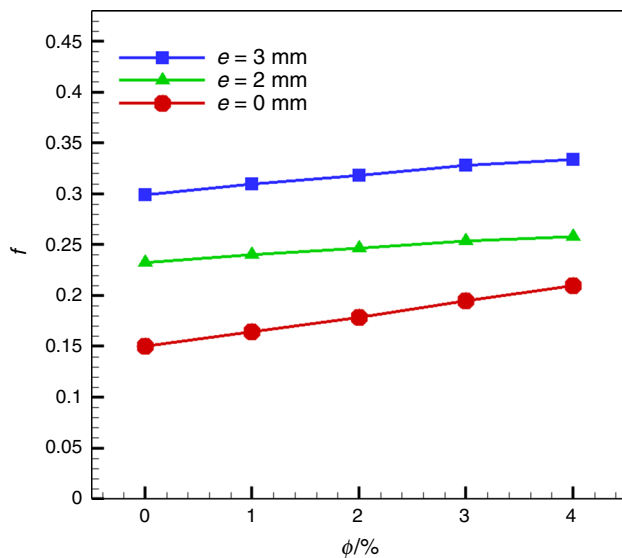


Fig. 6 Variations of friction factor with  $\phi$  at  $Re = 12,000$

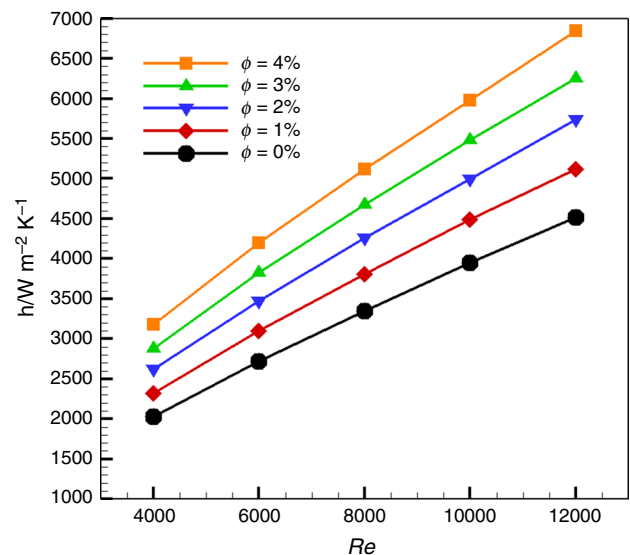


Fig. 8 Variations of HTC with  $Re$  for different values of  $\phi$  at  $e = 3$

$$u = 0, v = 0, w = 0, T = 298 \text{ K} \tag{34}$$

• At outlet:

$$\frac{\partial u}{\partial x} = 0, \frac{\partial v}{\partial x} = 0, \frac{\partial w}{\partial x} = 0, \frac{\partial T}{\partial x} = 0, \frac{\partial k}{\partial x} = 0, \frac{\partial \omega}{\partial x} = 0 \tag{35}$$

### Numerical method

A finite volume technique (SIMPLE algorithm) is employed to resolve the equations along the related boundary conditions [40]. The discretization of all governing equations is performed by using a second-order upwind differencing method. The iterative process stops when residuals reach less than  $10^{-6}$ . It should be men-

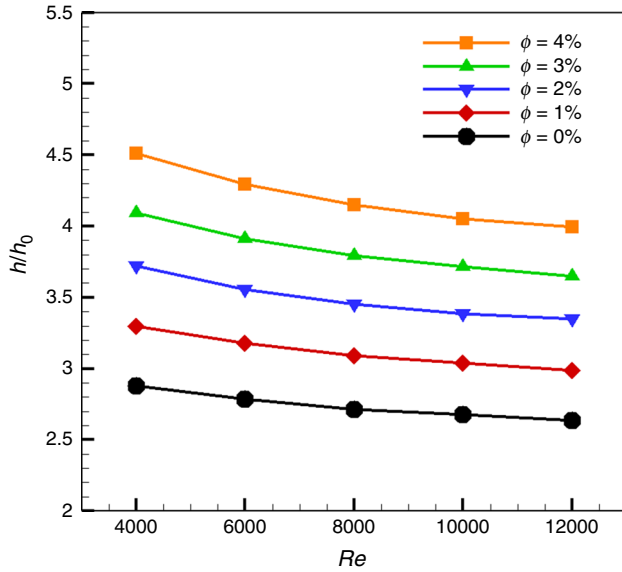


Fig. 9 Variations of dimensionless heat transfer coefficient augmentation with  $Re$  for different values of  $\phi$  at  $e = 3$

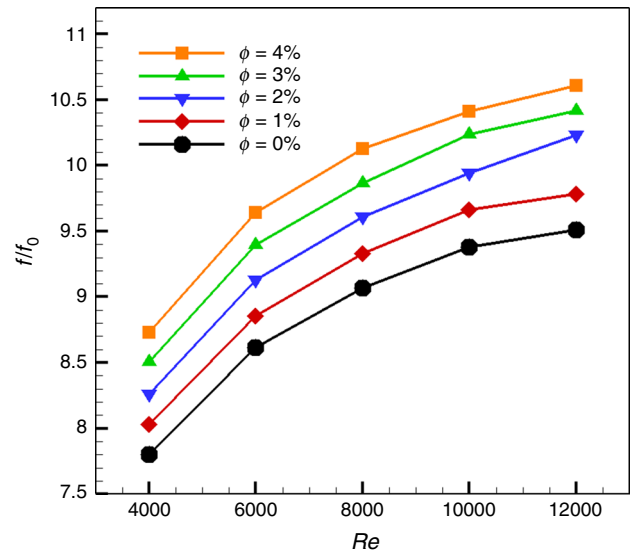


Fig. 11 Variations of dimensionless friction factor with  $Re$  for different values of  $\phi$

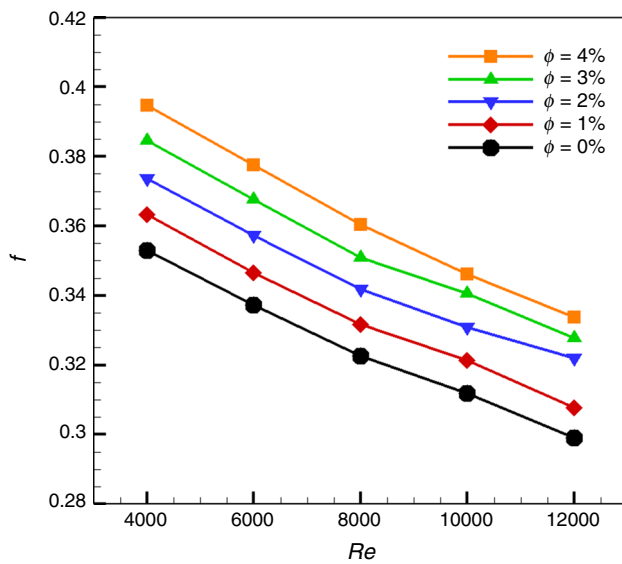


Fig. 10 Variations of friction factor with  $Re$  for different values of  $\phi$  at  $e = 3$

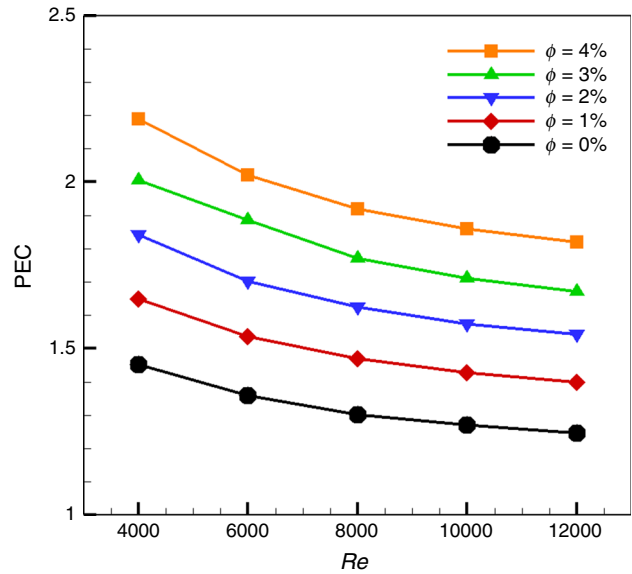


Fig. 12 Variations of performance evaluation criterion (pec) with  $Re$  for different values of  $\phi$  at  $e = 3$



tioned that the ANSYS Fluent software is used to simulate this problem.

### Grid independence test and validation

Grid distribution is displayed in Fig. 2. As an assumption in the SST  $k - \omega$  model,  $y^+$  should be less than unity around the surfaces. Values of  $y^+$  less than unity indicate that the grid is small sufficient to capture the laminar sublayer. The values of  $y^+$  are checked around the surfaces in this problem, and they were less than unity for all cases.

The grid independence evaluation was accomplished by considering four different mesh sizes as shown in Fig. 3. As shown, the difference between the friction factor of grid numbers for 3,000,000 and 6,000,000 is about 0.48%, which is insignificant. This difference for Nusselt number is about 0.09% which is acceptable. Accordingly, the mesh number of 3,000,000 was selected as the optimal mesh size for the study.

To evaluate the accuracy of the present numerical scheme, the findings obtained by the present work were benchmarked with the experimental findings of former studies. Figure 4a and b shows the comparison between the current numerical results and experimental results [11] for a tube fitted by the helical screw-tape without core-rod inserts (for  $e = 0$ ). It can be observed that the present numerical outcomes have a small deviation from the experimental results. Figure 4a shows the variation of  $Nu_{ave}$  with  $Re$ . The average relative error is about 6%. Figure 4b shows the variation of friction factor with  $Re$ . The average relative error is about 14%.

## Results and discussion

The effects of eccentricity and  $\phi$  on thermal-hydraulic performance containing heat transfer coefficient, friction factor and PEC are discussed.

Figure 5 shows the variations of HTC with  $\phi$  for three eccentricity values, at a constant Reynolds number, i.e., 12,000. As shown, the HTC enhances with an increase in  $\phi$  almost linearly. With increasing the volume fraction from 0 to 4%, the heat transfer coefficient enhances up to 51% for maximum eccentricity ( $e = 3$  mm). This enhancement for minimum eccentricity ( $e = 0$  mm) is 37%. Heat transfer coefficient is directly proportional with thermal conductivity, Reynolds and Prandtl numbers. Therefore, at a constant  $Re$ , we need focus on the variations of thermal conductivity and  $Pr$  number with NP volume fraction which affect the magnitude of HTC. By adding NPs to the base liquid, the effective thermal conductivity enhances. On the other hand, the value of  $Pr$  (i.e.,  $\frac{\mu_{cp}}{k}$ ) reduces by

particle loading (based on the properties given in Table 1). However, the enhancement in thermal conductivity can neutralize the reduction in  $Pr$  number because the HTC is a function of  $Pr^n$  where  $n$  is less than 1; therefore, the outcome is heat transfer coefficient amelioration.

Figure 6 shows the variations of  $f$  with solid volume fractions for three eccentricity values, for  $Re = 12,000$ . It shows that  $f$  increases with the addition of particles. The value of  $f$  increases about 11% for  $e = 2$  and  $e = 3$ , and about 40% for  $e = 0$ .

The effect of  $\phi$  on PEC is disclosed in Fig. 7. It is worth to mention that to achieve a precise consequence about the overall efficiency of the heat exchanger; it is needful to evaluate the pressure drop and the heat transfer in the heat exchanger, simultaneously. A Performance Evaluation Criterion (PEC) aids the designer to choose the best option based on the first law of thermodynamic viewpoint. Figure 7 shows that PEC values are higher than 1 so all these cases are acceptable and it means that using  $Al_2O_3$ /water NF in a tube with eccentric helical screw-tape at a constant pumping power leads to improve HTC. The PEC value improves about 46% by increasing in  $\phi$  in the range of 0–4% for  $e = 3$ . This improvement for minimum eccentricity value ( $e = 0$ ) is about 22%.

Figure 8 shows variations of HTC against  $Re$  for different solid volume fraction of NPs at  $e = 3$ . As shown in this figure, heat transfer coefficient enhances with an increase in  $Re$  for all values of  $\phi$ . There are 123%, 120%, 119%, 117% and 115% increments in the HTC for the cases of  $\phi = 0, 1, 2, 3$ , and 4 when the  $Re$  is increased from 4000 to 12,000. Moreover, the HTC increases when  $\phi$  increased for all values of  $Re$ . There are 57%, 54%, 53%, 51.3% and 51.5% improvements in HTC for  $Re = 4000, 6000, 8000, 10,000$ , and 12,000 when  $\phi$  increased from 0 to 4. Indeed, adding NPs helps to the augmentation of heat transfer coefficient about 1.5 times but this augmentation is higher in low  $Re$ .

Two dimensionless coefficients are defined to show the increase in HTC and  $f$  created by employing the heat transfer enhancement technique compared with plain tube ( $h/h_0$  and  $f/f_0$ ) where the subscript of “0” stands for HTC and  $f$  of the plain tube. It is shown in Fig. 9 that all values of  $h/h_0$  are greater than one which demonstrates the high heat transfer enhancement compared with plain tube case. It also shows that using  $Al_2O_3$ /water NF with eccentric helical inserts have higher heat transfer enhancement in lower  $Re$ .

The variations of friction factor against  $Re$  for different values of  $\phi$  at  $e = 3$  are shown in Fig. 10. As shown in this figure, friction factor decreases with an increase in  $Re$  for all values of solid volume fraction. It also shows that adding NPs leads to increase friction factor. This increase

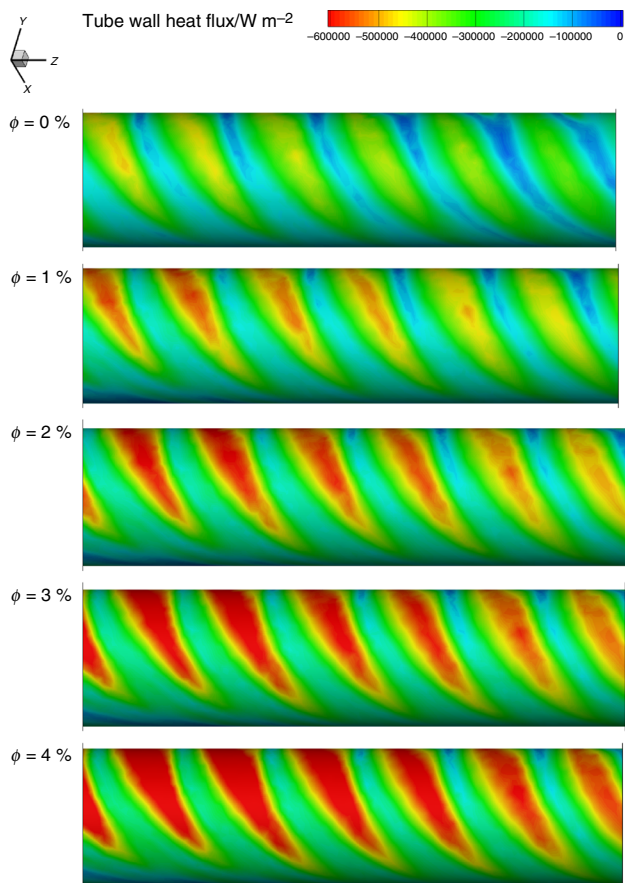


Fig. 13 The effects of  $\phi$  on tube wall heat flux contours at  $e = 3$ ,  $Re = 12,000$

for different all Reynolds number is 3–11.7% for solid volume fraction of 1–4%.

The dimensionless friction factor  $f/f_0$  is provided in Fig. 11. It shows that  $f/f_0$  for all cases increases with the increase in  $Re$ .

Figure 12 shows the variation of PEC against  $Re$  for different values of  $\phi$  at  $e = 3$ . According to the definition of this parameter, when the value of PEC is greater than unity it implies that using helical screw-tape is advantageous by considering both HTC and  $f$ . As seen, the value of PEC is greater than one independent of  $Re$  number and NF concentration. It means that although using helical screw-tape leads to an increase in the pressure drop, the heat transfer enhancement neutralizes it, and consequently, the PEC becomes greater than one. With increasing the volume fraction, the amount of PEC increases too, therefore, it can be concluded that adding NPs to the base fluid mainly leads to heat transfer augmentation and undesirable effects of friction factor growth is not dominant. The higher value of PEC at low Reynolds numbers can be described based on

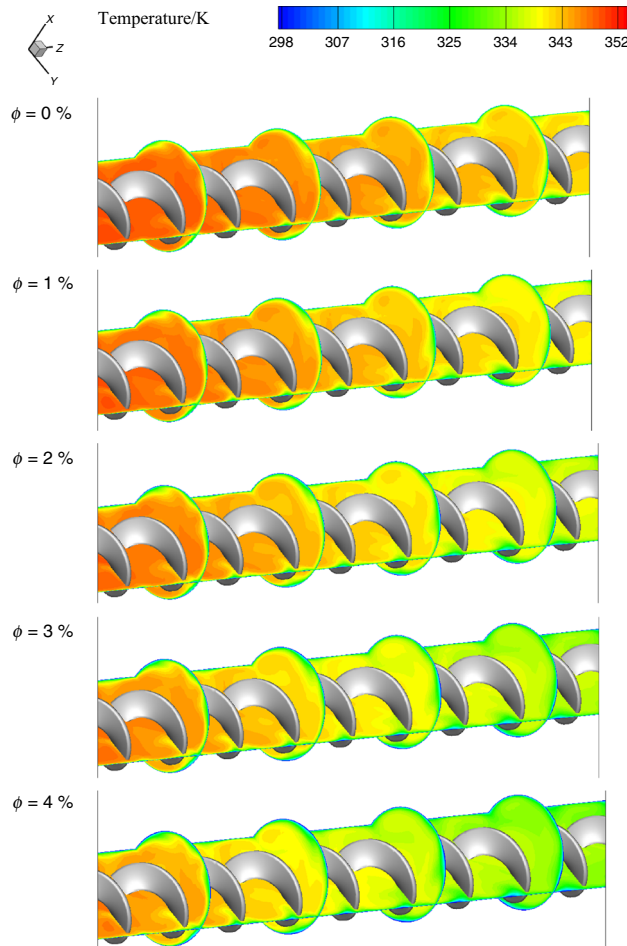
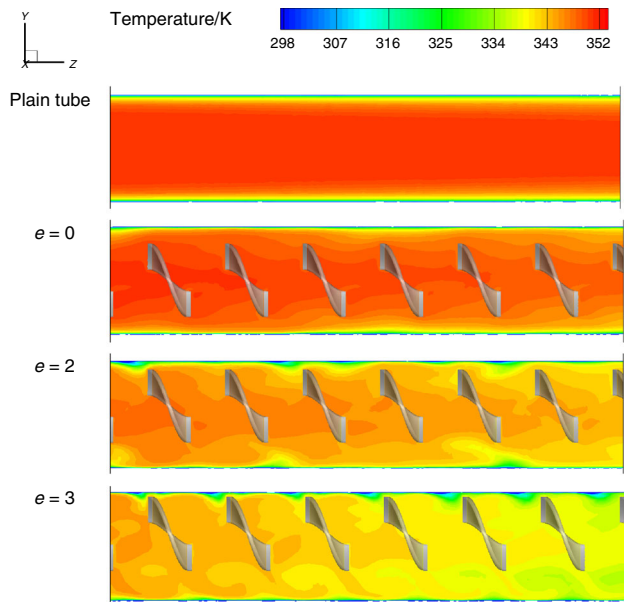


Fig. 14 The effects of  $\phi$  on temperature distribution contours at  $e = 3$ ,  $Re = 12,000$

Figs. 9 and 11. As seen, the rate of changes for both HTC and  $f$  ratios is greater at low  $Re$  numbers.

Figure 13 shows the effect of  $\phi$  on tube wall heat flux contours at  $e = 3$  and  $Re = 12,000$ . As shown in this figure, the tube wall heat flux increases by increasing in  $\phi$ . The main reasons were discussed earlier. It can be seen that the maximum wall heat flux is occurred on the tube wall in which helical direction that helical screw-tape swirls the flow. To determine the heat flux augmentation on the tube wall for each case (compared to plain tube), the dimensionless parameter  $q/q_0$  is calculated. For the cases shown in Fig. 13, this ratio is 3.53, 3.91, 4.28, 4.56 and 4.91 for  $\phi = 0, 1, 2, 3$  and  $4\%$ , respectively. Figure 14 shows the influence of  $\phi$  on temperature field at  $e = 3$  and  $Re = 12,000$ . As shown in this figure, the level of temperature in the domain tends to decrease when  $\phi$  increases. Finally, it leads to the decrease in outlet temperature of tube and better heat transfer performance of HE.



**Fig. 15** The effects of eccentricity on temperature contours at  $\phi = 4\%$  and  $Re = 12,000$

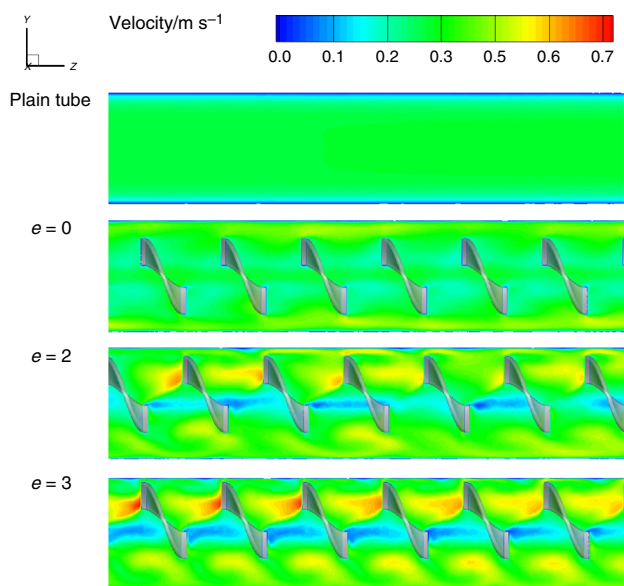


**Fig. 16** The effects of eccentricity on velocity contours at  $\phi = 4\%$  and  $Re = 12,000$

The effects of increases in eccentricity on temperature and velocity fields are shown in Figs. 15 and 16. It is seen that at  $\phi = 4\%$  and  $Re = 12,000$ , the heat transfer diffusion increases with an increase in the eccentricity value. The improvement in heat diffusion is due to the fact that with increasing the eccentricity the velocity profile becomes non-uniform in upper and lower halves (in concentric case is uniform since the effect of gravity is neglected). In the

half that the gap between the insert and the tube is smaller, forced convection intensity increases and the transfer of heat via convection to other areas of tube better happens through vorticities formed in the flow. In other words, mixing rate is more when eccentricity is higher; therefore, the rate of heat diffusion increases.

## Conclusions

Optimizing the efficacy of solar collectors and photovoltaic thermal (PV/T) systems, which their use is developing in buildings, will efficiently help to achieve zero-energy buildings. For this purpose, improving the efficiency of heat exchangers as the main part of solar collectors and PV/T systems is crucial. In this paper, the first law of thermodynamic was employed to evaluate the effects of helical screw-tape turbulator and NF in an HE tube for turbulent regime. The effects of eccentricity and  $\phi$  on thermal-hydraulic performance including HTC, friction factor and PEC were investigated. The main findings of this study can be listed as:

- The heat transfer coefficient increases with increasing of  $\phi$ . Adding NPs to working fluid has better influence when eccentric helical screw-tape is used instead of concentric helical screw-tape.
- The HTC rises with increasing the eccentricity as the turbulator with higher eccentricity causes a better temperature distribution.
- The friction factor increases with increasing of  $\phi$ . This increase is about 3–11% for volume fractions 1–4%.
- The PEC value is obtained about 1.2–1.4 for  $\phi = 0\%$  and 1.8–2.2 for  $\phi = 4\%$ . The higher PEC values are associated with lower  $Re$ .
- The PEC values improve about 57%, 55%, 53%, 50% and 48% by increasing  $\phi$  from 0 to 4% for Reynolds numbers of 4000, 6000, 8000, 10,000, and 12,000, respectively.
- The wall heat flux increases as  $\phi$  increases. The maximum wall heat flux is occurred on the tube wall in the path that helical screw-tape swirls flow.

The present work suggests the simultaneous usage of NFs and inserts to enhance the solar energy-based systems.

**Acknowledgements** This research was supported by the Office of the Vice Chancellor for Research, Ferdowsi University of Mashhad, under Grant No. 46494.

## References

1. Sun Y, Huang G, Xu X, Lai ACK. Building-group-level performance evaluations of net zero energy buildings with non-



- collaborative controls. *Appl Energy*. 2018;212:565–76. <https://doi.org/10.1016/j.apenergy.2017.11.076>.
2. Huang P, Huang G, Sun Y. Uncertainty-based life-cycle analysis of near-zero energy buildings for performance improvements. *Appl Energy*. 2018;213:486–98. <https://doi.org/10.1016/j.apenergy.2018.01.059>.
  3. Herrando M, Markides CN, Hellgardt K. A UK-based assessment of hybrid PV and solar-thermal systems for domestic heating and power: system performance. *Appl Energy*. 2014;122:288–309. <https://doi.org/10.1016/j.apenergy.2014.01.061>.
  4. Herrando M, Markides CN. Hybrid PV and solar-thermal systems for domestic heat and power provision in the UK: techno-economic considerations. *Appl Energy*. 2016;161:512–32. <https://doi.org/10.1016/j.apenergy.2015.09.025>.
  5. Bellos E, Tzivanidis C. Investigation of a star flow insert in a parabolic trough solar collector. *Appl Energy*. 2018;224:86–102. <https://doi.org/10.1016/j.apenergy.2018.04.099>.
  6. Bhattacharyya S, Chattopadhyay H, Haldar A. Design of twisted tape turbulator at different entrance angle for heat transfer enhancement in a solar heater. *Beni-Suef Univ J Basic Appl Sci*. 2017;7:118–26. <https://doi.org/10.1016/j.bjbas.2017.08.003>.
  7. Song X, Dong G, Gao F, Diao X, Zheng L, Zhou F. A numerical study of parabolic trough receiver with nonuniform heat flux and helical screw-tape inserts. *Energy*. 2014;77:771–82. <https://doi.org/10.1016/j.energy.2014.09.049>.
  8. Sheikholeslami M, Gorji-Bandpy M, Ganji DD. Effect of discontinuous helical turbulators on heat transfer characteristics of double pipe water to air heat exchanger. *Energy Convers Manag*. 2016;118:75–87. <https://doi.org/10.1016/j.enconman.2016.03.080>.
  9. Chang C, Peng X, Nie B, Leng G, Li C, Hao Y, et al. Heat transfer enhancement of a molten salt parabolic trough solar receiver with concentric and eccentric pipe inserts. *Energy Procedia*. 2017;142:624–9. <https://doi.org/10.1016/j.egypro.2017.12.103>.
  10. Lim KY, Hung YM, Tan BT. Performance evaluation of twisted-tape insert induced swirl flow in a laminar thermally developing heat exchanger. *Appl Therm Eng*. 2017;121:652–61. <https://doi.org/10.1016/j.applthermaleng.2017.04.134>.
  11. Eiamsa-ard S, Promvong P. Heat transfer characteristics in a tube fitted with helical screw-tape with/without core-rod inserts. *Int Commun Heat Mass Transf*. 2007;34:176–85. <https://doi.org/10.1016/j.icheatmasstransfer.2006.10.006>.
  12. Zhang X, Liu Z, Liu W. Numerical studies on heat transfer and friction factor characteristics of a tube fitted with helical screw-tape without core-rod inserts. *Int J Heat Mass Transf*. 2013;60:490–8. <https://doi.org/10.1016/j.ijheatmasstransfer.2013.01.041>.
  13. Rashidi S, Zade NM, Esfahani JA. Thermo-fluid performance and entropy generation analysis for a new eccentric helical screw tape insert in a 3D tube. *Chem Eng Process Process Intensif*. 2017. <https://doi.org/10.1016/j.cep.2017.03.013>.
  14. Liu X, Li C, Cao X, Yan C, Ding M. Numerical analysis on enhanced performance of new coaxial cross twisted tapes for laminar convective heat transfer. *Int J Heat Mass Transf*. 2018;121:1125–36. <https://doi.org/10.1016/j.ijheatmasstransfer.2018.01.052>.
  15. Moghadas N, Akar S, Rashidi S, Abolfazli J. Thermo-hydraulic analysis for a novel eccentric helical screw tape insert in a three dimensional tube. *Appl Therm Eng*. 2017;124:413–21. <https://doi.org/10.1016/j.applthermaleng.2017.06.036>.
  16. Mahian O, Kolsi L, Amani M, Estellé P, Ahmadi G, Kleinstreuer C, et al. Recent advances in modeling and simulation of nanofluid flows-part I: fundamentals and theory. *Phys Rep*. 2018. <https://doi.org/10.1016/j.physrep.2018.11.004>.
  17. Mahian O, Kolsi L, Amani M, Estellé P, Ahmadi G, Kleinstreuer C, et al. Recent advances in modeling and simulation of nanofluid flows-part II: applications. *Phys Rep*. 2018. <https://doi.org/10.1016/j.physrep.2018.11.003>.
  18. Bellos E, Tzivanidis C. A review of concentrating solar thermal collectors with and without nanofluids. *J Therm Anal Calorim*. 2018. <https://doi.org/10.1007/s10973-018-7183-1>.
  19. Wei H, Nor X, Che A, Najafi SG. Recent state of nanofluid in automobile cooling systems. *J Therm Anal Calorim*. 2018. <https://doi.org/10.1007/s10973-018-7477-3>.
  20. Sopian K, Alwaeli AHA, Najah A. Thermodynamic analysis of new concepts for enhancing cooling of PV panels for grid-connected PV systems. *J Therm Anal Calorim*. 2018. <https://doi.org/10.1007/s10973-018-7724-7>.
  21. Rashidi S, Mahian O, Languri EM. Applications of nanofluids in condensing and evaporating systems: a review. *J Therm Anal Calorim*. 2018;131:2027–39. <https://doi.org/10.1007/s10973-017-6773-7>.
  22. Khanafer K, Vafai K. A review on the applications of nanofluids in solar energy field. *Renew Energy*. 2018;123:398–406. <https://doi.org/10.1016/j.renene.2018.01.097>.
  23. Khanafer K, Vafai K. Applications of nanofluids in porous medium: a critical review. *J Therm Anal Calorim*. 2018. <https://doi.org/10.1007/s10973-018-7565-4>.
  24. Raei B, Shahraki F, Jamialahmadi M, Peyghambarzadeh SM. Experimental study on the heat transfer and flow properties of  $\gamma$ - $\text{Al}_2\text{O}_3$ /water nanofluid in a double-tube heat exchanger. *J Therm Anal Calorim*. 2017;127:2561–75. <https://doi.org/10.1007/s10973-016-5868-x>.
  25. Sundar LS, Singh MK, Punnaiah V, Sousa ACM. Experimental investigation of  $\text{Al}_2\text{O}_3$ /water nanofluids on the effectiveness of solar flat-plate collectors with and without twisted tape inserts. *Renew Energy*. 2018;119:820–33. <https://doi.org/10.1016/j.renene.2017.10.056>.
  26. Syam Sundar L, Singh MK, Sousa ACM. Heat transfer and friction factor of nanodiamond-nickel hybrid nanofluids flow in a tube with longitudinal strip inserts. *Int J Heat Mass Transf*. 2018;121:390–401. <https://doi.org/10.1016/j.ijheatmasstransfer.2017.12.096>.
  27. Sheikholeslami M, Jafaryar M, Li Z. Nanofluid turbulent convective flow in a circular duct with helical turbulators considering CuO nanoparticles. *Int J Heat Mass Transf*. 2018;124:980–9. <https://doi.org/10.1016/j.ijheatmasstransfer.2018.04.022>.
  28. Esmaeilzadeh E, Almohammadi H, Nokhosteen A, Motezaker A, Omrani AN. Study on heat transfer and friction factor characteristics of  $\gamma$ - $\text{Al}_2\text{O}_3$ /water through circular tube with twisted tape inserts with different thicknesses. *Int J Therm Sci*. 2014;82:72–83. <https://doi.org/10.1016/j.ijthermalsci.2014.03.005>.
  29. Sheikholeslami M, Jafaryar M, Ganji DD, Li Z. Exergy loss analysis for nanofluid forced convection heat transfer in a pipe with modified turbulators. *J Mol Liq*. 2018;262:104–10. <https://doi.org/10.1016/j.molliq.2018.04.077>.
  30. Bellos E, Tzivanidis C, Tsimpanos D. Enhancing the performance of parabolic trough collectors using nanofluids and turbulators. *Renew Sustain Energy Rev*. 2018;91:358–75. <https://doi.org/10.1016/j.rser.2018.03.091>.
  31. Akyürek EF, Geliş K, Şahin B, Manay E. Experimental analysis for heat transfer of nanofluid with wire coil turbulators in a concentric tube heat exchanger. *Results Phys*. 2018;9:376–89. <https://doi.org/10.1016/j.rinp.2018.02.067>.
  32. Zheng L, Xie Y, Zhang D. Numerical investigation on heat transfer performance and flow characteristics in circular tubes with dimpled twisted tapes using  $\text{Al}_2\text{O}_3$ -water nanofluid. *Int J Heat Mass Transf*. 2017;111:962–81. <https://doi.org/10.1016/j.ijheatmasstransfer.2017.04.062>.

33. Rashidi S, Eskandarian M, Mahian O, Poncet S. Combination of nanofluid and inserts for heat transfer enhancement. *J Therm Anal Calorim*. 2018. <https://doi.org/10.1007/s10973-018-7070-9>.
34. Albojamal A, Vafai K. Analysis of single phase, discrete and mixture models, in predicting nanofluid transport. *Int J Heat Mass Transf*. 2017;114:225–37. <https://doi.org/10.1016/j.ijheatmasstransfer.2017.06.030>.
35. Bovand M, Rashidi S, Esfahani JA. Enhancement of heat transfer by nanofluids and orientations of the equilateral triangular obstacle. *Energy Convers Manag*. 2015;97:212–23. <https://doi.org/10.1016/j.enconman.2015.03.042>.
36. Parsazadeh M, Mohammed HA, Fathinia F. Influence of nanofluid on turbulent forced convective flow in a channel with detached rib-arrays. *Int Commun Heat Mass Transf*. 2013;46:97–105. <https://doi.org/10.1016/j.icheatmasstransfer.2013.05.006>.
37. Menter FR. Two-equation eddy-viscosity turbulence models for engineering applications. *AIAA*. 1994;32:1598–605.
38. Webb RL. Performance evaluation criteria for use of enhanced heat transfer surfaces in heat exchanger design. *Int J Heat Mass Transf*. 1981;24:715–26. [https://doi.org/10.1016/0017-9310\(81\)90015-6](https://doi.org/10.1016/0017-9310(81)90015-6).
39. Eiamsa-Ard S, Promvong P. Thermal characteristics in round tube fitted with serrated twisted tape. *Appl Therm Eng*. 2010;30:1673–82. <https://doi.org/10.1016/j.applthermaleng.2010.03.026>.
40. Patankar SV. Numerical heat transfer and fluid flow. New York: Hemisphere; 1980.

**Publisher's Note** Springer Nature remains neutral with regard to jurisdictional claims in published maps and institutional affiliations.